HHS Public Access

Author manuscript

Nat Neurosci. Author manuscript; available in PMC 2021 May 09.

Published in final edited form as:

Nat Neurosci. 2020 December ; 23(12): 1550–1554. doi:10.1038/s41593-020-00732-1.

A cerebello-olivary signal for negative prediction error is sufficient to cause extinction of associative motor learning

Olivia A. Kim, **Shogo Ohmae**, **Javier F. Medina**

Department of Neuroscience, Baylor College of Medicine, Houston, TX 77030

Abstract

The brain generates negative prediction error (NPE) signals to trigger extinction, a type of inhibitory learning that is responsible for suppressing learned behaviors when they are no longer useful. Neurons encoding NPE have been reported in multiple brain regions. Here, we use an optogenetic approach to demonstrate that GABAergic cerebello-olivary neurons can generate a powerful NPE signal, capable of causing extinction of conditioned motor responses on its own.

Keywords

Rescorla-Wagner; fear conditioning; PTSD; inferior olive; climbing fiber; complex spike; cerebellum

When an expected event does not happen, the brain generates a negative prediction error (NPE) signal that is used to optimize our actions by triggering neural mechanisms of extinction[1], an adaptive form of inhibitory learning responsible for the gradual suppression and eventual elimination of maladaptive behaviors[2]. Previous work has suggested that neurons in the inferior olive (IO) encode an NPE signal during cerebellar-dependent learning tasks[1,3]. Support for this hypothesis comes from eyeblink conditioning studies showing that IO neurons are briefly inhibited when an aversive eye puff is unexpectedly omitted[1,4,5]. However, we do not know if this reportedly brief inhibition of the IO is *sufficient* for extinction of the eyeblink response (conditioned response, CR), partly because previous attempts to examine this question have relied on electrical stimulation, pharmacological inactivation or lesions to suppress IO activity[6–8]. Because these manipulations are not cell type-specific and in some cases lack temporal precision, they can result in abnormal activation of mossy fiber inputs to the cerebellum[8], or cause widespread destabilization of

Correspondence to: Javier Medina, Department of Neuroscience, Baylor College of Medicine, One Baylor Plaza, Houston, TX 77030, Javier.Medina@bcm.edu.

AUTHOR CONTRIBUTIONS

O.K. & J.M. designed the experiments. J.M. supervised the project. O.K. performed virus injection and optical fiber implant surgeries, and conducted all behavior/optogenetics experiments. S.O. performed all electrophysiology-related surgery and experiments. O.K. analyzed and curated all original data collected for this publication. S.O. curated data included from a previous publication. O.K. & J.M. wrote the original draft of the paper. J.M., O.K., & S.O. revised and edited the paper.

CONFLICT OF INTEREST

The authors declare no competing financial interests.

olivo-cerebellar circuits that leads to general deficits in motor performance and has made previous experimental results difficult to interpret[9].

We used an optogenetic approach to inhibit eye puff-driven responses in the IO of mice (Fig. 1). Because direct inhibition of IO neurons with hyperpolarizing opsins was impractical in our experiments (Extended Data Fig. 1), we opted for an approach that exploits the natural circuitry of the brain. A virus (AAV5-hSyn-hChR2(E123A)-EYFP) was injected into the right cerebellar nuclei, resulting in expression of ChR2 in somata of the cerebellar nucleus neurons (Fig. 1a–d), and in the GABAergic axon terminals of projections from the cerebellar nuclei to the contralateral IO (cerebellar nucleo-olivary pathway; CN_{IO}, Fig. 1e–h). To validate the approach we delivered airpuffs to the right eye while simultaneously photostimulating the inhibitory CN_{IO} pathway via an optical fiber implanted above the left IO at the level of the dorsal accessory olive (Fig. 1e; see Extended Data Fig. 2 for a diagram of the anatomy; Extended Data Fig. 3 for histological analysis of optical fiber placement). This approach likely confines the effects of photostimulation to the IO because non-CN_{IO} neurons expressing ChR2 around the AAV-injection site are too far to be directly activated by the laser light (>2.5 mm), and because the axons of CN_{IO} neurons have no known collaterals and are thought to project only to the IO[10]. The responses of individual IO neurons to the airpuff, which were measured by recording climbing fiber-driven complex spikes in Purkinje cells (‘Record’, Fig. 1a), were strongly suppressed by CN_{IO}-terminal photostimulation (Fig. 1i–l), although the IO was not always completely silenced and a small response remained in some cases (Fig. 1l). When the suppression of eye puff-driven responses resulted in a pause of IO firing, it was often followed by a rebound in the post-stimulation period (Fig. 1k,l), reminiscent of the pattern of IO activity previously observed when an expected eye puff is omitted during normal extinction trials[5] (Extended Data Fig. 4). We will refer to photostimulation of GABAergic CN_{IO} terminals in the IO as “CN_{IO} stimulation” for the remainder of this paper.

To test whether CN_{IO} stimulation can serve as a negative prediction error (NPE) and effectively drive extinction, mice expressing ChR2-EYFP in CN_{IO} axon terminals were trained in an eyeblink conditioning task (‘ChR2’ mice; see Online Methods for task details). After the mice learned to make eyeblink CRs and performance stabilized (Fig. 2a,b; ‘Training’), we continued to deliver normal conditioning trials while adding a brief CN_{IO} stimulation pulse during the eye puff (200 ms pulse starting 20 ms before airpuff trigger, Fig. 2a,b; ‘ChR2’). Over multiple sessions of CN_{IO} stimulation, ChR2 mice showed a gradual decay in CR probability (Fig. 2b) and CR amplitude (Fig. 2c–d). This decline in CR performance was also observed in wildtype mice undergoing extinction training with unpaired stimulus presentations (‘WT’ mice; Fig. 2e–f), and had a similar time course (Fig. 2b). Further analysis of CR performance in the ChR2 mice revealed three additional behavioral hallmarks of normal extinction: First, ChR2 mice made more CRs at the beginning of a CN_{IO} stimulation session than at the end of the preceding session (Extended Data Fig. 5a–b), a clear sign of spontaneous recovery behavior commonly observed during normal extinction (Extended Data Fig. 5c–d). Second, when normal conditioning sessions resumed after 10 days of CN_{IO} stimulation, ChR2 mice showed retention of the extinction memory on the first day of reacquisition, making very few CRs initially (Fig. 2b), and performing at a lower CR amplitude than in the last baseline day (Fig. 2h). Third, with

further conditioning ChR2 mice then displayed ‘savings’ (Extended Data Fig. 5e–f): CRs were relearned faster than during initial acquisition (see Extended Data Fig. 5g–h for a comparison with savings after normal extinction with unpaired stimulus presentations in WT mice).

Our analyses suggest that the gradual decay in CR performance of ChR2 mice in Fig. 2 is the result of an extinction process. We performed 5 control experiments to rule out alternative explanations: (1) Mice expressing EYFP or no fluorescent protein in CN_{IO} axon terminals (‘Control’ mice; Extended Data Fig. 3 for histological analysis) showed no effects of photostimulation on CR probability (Fig. 2b). Thus, the light or the heat generated by the photostimulation did not cause ChR2 mice to stop making CRs. (2) Following the optogenetic experiments, all ChR2 mice reacquired the CR and attained pre-stimulation performance levels (Fig. 2b,g–h; ‘Training’ vs ‘Retraining’), indicating that CN_{IO} stimulation did not cause permanent damage to the olivo-cerebellar circuits that are critical for eyeblink conditioning[11]. (3) Impairments in processing the eye puff stimulus could also be ruled out because CN_{IO} stimulation had no effect on the amplitude of reflexive blinks in ChR2 mice (Extended Data Fig. 6a,b), and although its duration was shortened (Extended Data Fig. 6c), similar changes in reflex duration did not affect CR probability during normal training (Extended Data Fig. 6d,e). (4) CN_{IO} stimulation did not weaken the ongoing motor drive for the CR directly because ChR2 mice that received CN_{IO} stimulation throughout the entire CR window (200 ms before eye puff) made more frequent and bigger CRs (Extended Data Fig. 7a–f), and produced reflexive eyelid movements after the tone that were more vigorous than normal, including bigger β-startles (Extended Data Fig. 7g–i) with shortened latency (Extended Data Fig. 7j). (5) Finally, the two experiments shown in Fig. 3 demonstrate that the repeated delivery of brief but frequent CN_{IO} stimulation pulses did not cause dysregulation of activity in downstream Purkinje cells, which is known to produce impairments in CRs that can be mistaken for extinction learning[9]. First, the cerebellum remained functional in ChR2 mice that received CN_{IO} stimulation 350 ms after the eye puff stimulus in every conditioning trial (Fig. 3a), as evidenced by stable CR probability (Fig. 3b) and CR amplitude (Fig. 3c–e). Second, the firing rate of Purkinje cells whose climbing fiber responses to the eye puff were effectively suppressed by the optogenetic stimulation (Fig. 1l) remained stable across recording sessions with repeated CN_{IO} stimulation pulses (Fig. 3f).

We have shown that brief stimulation of GABAergic CN_{IO} neurons has minimal impact on ongoing motor performance but is an effective NPE signal, sufficient to cause ‘paradoxical’ extinction, i.e. mice learned to stop making CRs, leaving the cornea unprotected despite continued presentation of the aversive eye-puff stimulus. This effect is most likely the result of CN_{IO}-driven inhibition of the IO, because CN_{IO} neurons are thought to project only to the IO and do not have any known collaterals with direct access to the motor areas responsible for generating the eyeblink CR[10,11]. It may seem surprising that CN_{IO} stimulation, which has an inhibitory effect in IO neurons that fire at very low spontaneous rates to begin with (approximately 1 Hz)[12], can serve as a powerful NPE signal and have such profound effects on behavior. In this regard, the IO bears a striking resemblance to the midbrain dopamine system, where NPE signals for extinction in a variety of tasks are generated via inhibition of dopaminergic cells[13–15], which also have a low spontaneous firing rate that severely limits the range of NPE values that can be veridically represented[16]. Further experiments will be

needed to assess whether the dynamic range of NPE signals originating in the IO can be enhanced downstream in the cerebellar cortex, possibly by modulation of complex spike responses in Purkinje cell populations[12].

It is remarkable that mice learned to stop making CRs during CN_{IO} stimulation, even though this is a maladaptive change in behavior that leaves the cornea exposed at the time of the eye puff, and many neurons outside the IO must have been broadcasting error signals for promoting protective CRs. Indeed, error signals have been observed throughout the brain[1], including in many neurons of the cerebellum[17–20], which is the brain area responsible for making eyeblink CRs[11]. We do not know how all of these signals may interact to drive adaptive changes in behavior and optimize future performance. However, our results indicate that despite the multiplicity of error signals likely to be present in the brain during our experiments, NPE signals generated in the IO take precedence. Because CN_{IO} neurons are capable of profoundly reducing sensory-evoked responses in the IO, they appear to be ideally positioned to dictate which behaviors will ultimately be acquired or extinguished during cerebellar learning.

ONLINE METHODS

Please refer to Life Sciences Reporting Summary for additional information.

Animals.

All procedures were approved by the Baylor College of Medicine (BCM) Institutional Animal Care and Use Committee based on the guidelines of the US National Institutes of Health. Experiments were performed on male C57BL/6J mice at least 10 weeks of age (n = 23 mice) housed on a reverse light/dark cycle (8:00 AM-8:00 PM lights-off) in cages of up to 4 mice before surgery and singly-housed after surgery. Ambient temperature was maintained between 68–72 F, and ambient humidity was maintained between 30–70% RH. No statistical methods were used to pre-determine sample sizes, but our sample sizes were similar to those reported in previous publications[5, 14]. Mice were randomly allocated into different groups. Two mice were removed from the experiment because task performance failed to reach criterion during the training phase.

Surgery.

Procedures have been described previously[21]. In brief, mice were anesthetized with isoflurane (5% by volume in O_2 for induction, 1–2% by volume for maintenance; SurgiVet) and kept on a heating pad to maintain body temperature. Surgeries were carried out under sterile conditions, and mice received preoperative analgesia (0.02 mL 0.5% bupivacaine and 2% lidocaine, s.c. at incision site; 5 mg/kg meloxicam, s.c.). Fascia and obstructing muscle tissue were cleared from the skull through a midline incision, and the skull was leveled into the stereotaxic plane. Each mouse (n = 23 mice) received a head-plate implant, secured to the skull using 2 jeweler's screws (relative to bregma: AP −0.5 mm, ML ±1.3 mm) and C&B Metabond. The 5 mice used for extinction did not receive any further implants ('*WT*' group). All remaining mice (n = 18 mice) were implanted with an optical fiber (400 μm-diameter, constructed in-house using ThorLabs FP400URT, 0.22 NA) just dorsal of the left

DAO (relative to bregma: AP −6.6 mm, ML +0.2 mm, relative to skull surface at AP/ML target: −5.4 mm). Mice with fiber implants also received a virus injection (200 nL, 10 nL/min, Hamilton Neuros, 65458–02 with 30° bevel; WPI, UMP-3 pump) in the right AIP (relative to lambda: −2.0 mm AP, −1.9 mm ML, relative to dura mater surface at AP/ML target: −2.4 mm DV; 10° angle posterior to anterior). For 4 of the 18 mice ('*Control*' group), we injected AAV5-hSyn-EYFP (Karl Deisseroth, UNC Vector Core). For the remaining 14 mice ('*ChR2*' group), we injected AAV5-hSyn-hChR2(E123A)-EYFP (Karl Deisseroth, UNC Vector Core). In 4 of the 14 mice in the ChR2 group, we opened a craniotomy over the right cerebellar cortex to record eye puff-driven complex spikes in Purkinje cells (2.5 × 2.5 mm; protected by a 3D-printed chamber, NeuroNexus).

Stimulus control and behavioral monitoring.

Conditioning sessions were conducted inside of a sound-attenuating chamber. During all sessions, masking white noise was delivered in the background at 65 dB. Tone stimuli (500 ms duration, 10 kHz) were delivered via a speaker (Dell, AC511) positioned behind the mouse. Airpuffs were delivered via a pressure injector (ASI, MPPI-3) connected to plastic tubing terminating in a blunt-tipped, 23 G needle positioned 5 mm in front of the mouse's right eye. A high-speed monochrome camera (Allied Vision Technologies, GE680) recorded 200 fps videos of the right side of the face (i.e, ipsilateral to the virus injection site) under infrared (Bosch, EX12LED) illumination. During sessions with photostimulation, light was delivered using analog-controlled, 473 nm lasers (Blue Sky Research, FTEC2473) and 200 μm-diameter patch cables. Blue ambient illumination (5x, Uxcell a14122700ux0012 in series, 550 Ω resistance to ground, 5V 2A power supply) was present throughout all sessions to mask light escaping from the junction between the patch cable and implanted ferrule during photostimulation. Because the goal of our experiments was to examine learning processes that take place over consecutive days, the same stimulus presentations and experimental conditions were maintained constant for multiple sessions before switching to a different condition.

Acquisition of eyeblink conditioning.

Mice underwent 2 days of habituation training, during which they were head-fixed on top of a cylindrical treadmill and allowed to locomote freely, as they would be during all future experiments. At the beginning of all subsequent sessions, mice received a blink-eliciting airpuff (8.5 peak PSI, 30 ms trigger duration) to calibrate eyelid position measurements. On the first day of conditioning, up to 15 presentations of 10 kHz tones were delivered (60+ s ITI) at different volumes (65–95 dB) to find the lowest intensity that reliably evoked an eyelid startle in each mouse. This tone volume was used for the rest of the experiment. Conditioning sessions consisted of 100 tone + airpuff trials per day (200 ms ISI, 15–20 s ITI; 30 ms airpuff duration), unless mice exhibited signs of excessive stress and sessions were terminated early. After task acquisition (performance criterion of >60% conditioned responses [CR; see "Behavioral data analysis" below for CR criteria] on three consecutive days), airpuff intensity was systematically decreased in 9 of the mice, to shorten the duration of the reflex blink and examine the impact on CR probability. Before initiating either photostimulation or extinction sessions, the airpuff intensity was reset in all mice to just above threshold for maintaining >50% CRs, and kept at that level for at least 2 days to verity

that the duration of the reflex blink was ~200 ms and that conditioned responding was stable (±10% CRs).

Photostimulation experiments.

During photostimulation experiments, tone + airpuff stimuli continued to be presented as above, and a brief pulse of light (200 ms, 473 nm wavelength) was delivered via the implanted optical fiber at a particular time in every trial. We performed 3 experiments that were identical, except for the time in the trial at which the photostimulation pulse was delivered: 1) Photostimulation during puff (onset 20 ms before airpuff trigger), 2) Photostimulation after puff (onset 350 ms after the airpuff trigger, after tone & airpuff offset) 3) Photostimulation before puff (onset 200 ms before the airpuff trigger, simultaneous with tone onset). The same timing for the photostimulation pulse was used for up to 10 consecutive days. Between experiments with different photostimulation timings, mice were returned to normal conditioning trials to re-establish baseline performance. To estimate the level of irradiance reaching the DAO, we first calculated the light power at the base of the tether by taking into account the input laser power and discounting this value by the percent loss due to light transmission through each optical fiber. Then, for each mouse we measured the distance between the DAO and a lesion marking the tip of the optical fiber (marking lesion deliberately made at the end of the experiment by 30 s of 85 mW photostimulation), and used this measurement to estimate irradiance in the DAO based on the known degree of irradiance decay over distance in mammalian brain tissue[22]. Our estimates of irradiance in the DAO ranged from 7.57 mW/mm^2 to 30.59 mW/mm^2 (corresponding to 32.97–75.00 mW at the base of the tether in optical fibers with transmission efficiency values ranging from 76–92%). Note that, because the optical fiber tip was implanted just dorsal to the IO, which is >2mm ventral of and posterior to the cerebellar nuclei, light irradiance at the level of the AAV injection site would have been negligible (an estimated 0.34–0.75 mW/mm^2 in the caudal pole of the posterior interpositus, 0.25–0.50 mW/mm^2 in the eyeblink hotspot of the anterior interpositus). To examine reacquisition, after the last day of photostimulation all mice received 3–5 consecutive days of training with behavioral sessions consisting of 100 tone + airpuff trials.

Extinction experiment.

We used an unpaired stimulus protocol[23] to examine normal extinction in 5 wildtype mice that were not used for any of the photostimulation experiments. For 10 consecutive days, the mice received daily sessions with 200 trials each (7–10 s ITI). On odd-numbered trials, the tone was presented alone. On even-numbered trials, the airpuff was presented alone. This unpaired extinction protocol provides a more suitable comparison group than other extinction protocols based on just tone presentations because it degrades the contingency between the tone and the airpuff while maintaining the same total number of tone and airpuff presentations per session as in the experimental groups. To examine reacquisition, after the last day of extinction all mice received 3–5 consecutive days of additional training with behavioral sessions consisting of 100 tone + airpuff trials.

Behavioral data analysis.

Analyses were conducted using custom scripts written in MATLAB. Eyelid position was calculated for each video frame by counting the number of white pixels in a thresholded binary image of the eye and surrounding fur, as described previously[21]. Eyelid position is reported in units of the fraction eyelid closure (FEC) on a scale ranging from 0 (open) to 1 (closed). Eyelid velocities were computed by subtracting FEC in consecutive frames and dividing the differences by frame duration (5 ms). Trials with movement (FEC > 0.3) during the 200 ms baseline period before stimulus onset were excluded from analyses.

To assess the direct impact of our CN_{IO} stimulation on the motor circuits that drive different types of blinks, we analyzed the properties of both learned eyelid movements (*CR*, 120–200 ms from tone onset), as well as reflex eyelid movements made in response to the tone (*α-startle*, 0–50 ms from tone onset; *β-startle*, 50–120 ms from tone onset), and in response to the airpuff (*unconditioned reflex blink*, 200–800 ms from tone onset). β-startle amplitude was defined as FEC at 75 ms after tone onset, and β-startle latency was defined as time in the (50–120 ms) window at which eyelid position reached ≥0.05 FEC above baseline. CR amplitude was defined as mean FEC in the CR window (120–200 ms) minus the β-startle amplitude, to exclude non-associative startle-related blinking from CR measurements. CR probability was defined as the proportion of trials in which eyelid movement passed thresholds for blink speed (1 FEC/s) and blink size (measured at 180 ms after tone onset; 0.1 FEC for 14/19 mice, 0.2 FEC for 5/19 mice; thresholds selected based on individual mouse β-startle amplitudes). To prevent contamination from CRs, reflex blinks were measured in trials without any movements before the airpuff. Reflex blink amplitude was defined as peak FEC in the 150 ms after the airpuff trigger, and reflex blink duration was defined as the time the eyelid stayed >80% closed.

Single-unit recording.

Purkinje cell simple spikes (SSpks) and complex spikes (CSpks) were isolated using a tetrode (Thomas Recording, AN000968) mounted on a hydraulic microdrive (Narishige, MMO-220A) and driven into the cerebellar cortex of naïve mice using a micromanipulator (Narishige, SMM-100). Single-unit isolation was established and periocular airpuffs were delivered to verify that the isolated cell responded to the stimulus with a CSpk. Then, a repeating block design consisting of one airpuff trial, one photostimulation trial (200 ms duration, 473 nm wavelength, 8.12–30.59 mW/mm^2), and one trial with airpuff and photostimulation (airpuff trigger 20 ms after laser onset, same photostimulation parameters as above) was carried out until until isolation was lost (66–224 total trials). In addition, Extended Data Fig. 4 includes CSpk activity from a previously collected dataset[5], which contains recordings performed as described above (n = 6 C57bl6/J mice, n = 32 units), but collected during presentation of normal extinction trials in conditioned mice.

Single-unit data analysis.

SSpks and CSpks were sorted manually for 200+ ms preceding and 1000 ms following each trial. The different spike types were identified by their characteristic waveforms in Spike2, and trials with poor SSpk and CSpk isolation were excluded from further analyses. The presence of statistically significant CSpk rebounds after inhibition was assessed by

generating a bootstrapped distribution from the pre-trial baseline data of each individual neuron, using a case resampling procedure with replacement and the Monte Carlo algorithm. A neuron was classified as exhibiting a CSpk rebound if firing rate in the 50 ms after a pause was greater than 99% of the bootstrapped distribution.

Histology.

After mice with optical fiber implants completed the behavioral experiment, marking lesions were made via intense light stimulation through the optical fibers (Shanghai Laser & Optics Century Co., BL473T3–150FC, 85 mW for 30 s). Three days later, mice were euthanized and brains were extracted. Tissue was stored at 4 degrees C in 4% paraformaldehyde (Affymetrix, AAJ19943K2) overnight before being transferred to a 30% sucrose solution in PBS for 3–5 days. Tissue was sectioned at 50 μm thickness on a cryostat (Leica, CM1950) and alternating sections were either stained with red fluorescent Nissl (3.3% in PBS, ThermoFisher, N21482) or cresyl violet (0.5% cresyl violet and 0.3% glacial acetic acid in ddH_2O). Photomicrographs were captured using a Zeiss microscopy setup (Axio Imager microscope and ZEN software, blue edition) capable of imaging in epifluorescence and bright field modes, or a Nikon A1Rs confocal laser scanning microscope (NIS-elements Confocal and NIS-Elements Viewer for Windows Version 4).

Statistics and reproducibility.

Tests were performed in Matlab (version 2018b) and R (version 3.6.0, including external R packages: nparLD, coin, effsize. nlme, lsmeans, tidyverse, ggpubr, rstatix, car, multcompView, and sjstats). Where data distributions met the relevant assumptions (Mauchly's test for sphericity and Shapiro-Wilk test for normality of residuals for repeated measures ANOVA and for normality of test data for t-tests), we used the more sensitive, parametric test. When data met assumptions of the t-test and our purpose was to test the specific hypothesis that values in one group exceeded values in another group, a one-tailed t-test was used. Where data distributions violated the relevant assumptions, we used the corresponding non-parametric test (Friedman's ANOVA as an alternative to the repeated measures ANOVA, Wilcoxon's signed rank test as an alternative to the paired t-test, Wilcoxon's rank sum test as an alternative to the two-sample t-test). To compare rates of learning when the assumptions of a parametric, 2-way repeated measures ANOVA were violated, we performed a nonparametric analysis of longitudinal data using the F1-LD-F1 design implemented by the "nparLD" package in R. When Wald-type and ANOVA-type analyses revealed the same significant and non-significant results, the ANOVA-type statistics are reported. In order to accommodate differences in the number of days in each phase between mice, we examined performance on the last baseline day, manipulation days 1–4, and the final 2 manipulation days for our ANOVAs. Statistical analyses were also run on the complete dataset using the Skillings-Mack test – a repeated measures test that accommodates missing data without excluding datapoints. Skillings-Mack tests and ANOVAs revealed the same significant and non-significant results for the various experimental conditions, so we reported the results from the more commonly used statistical test in the main text of the paper. Family-wise α was maintained at 0.05 using the Bonferroni-Holm correction. Effect sizes for statistically significant results were measured

using Kendall's W (for Friedman repeated measures ANOVA) and Cohen's d (for paired t-tests, with paired samples with pooled standard deviation).

All electrophysiological and behavioral experiments with ChR2 mice were conducted over 2 rounds, with each experiment conducted on a different group of mice and producing similar results (Figs. 1–3; Extended Data Figs. 3–7). Confocal microscopy (Nikon AR1s), for which data from a representative mouse is shown in Figure 1, was conducted for 2/14 mice injected with AAV5-hSyn-hChR2(E123A)-EYFP and showed similar results across animals (1 confocal stack taken per mouse). Tissue from all mice was imaged via quasi-confocal microscopy (Zeiss Axio-Imager) and showed the same pattern of expression (20–30, 5x tiled photomicrographs at the level of the cerebellar nucleus and inferior olive taken per mouse). Representative images from 11/14 mice injected with AAV5-hSyn-hChR2(E123A)-EYFP are shown in Extended Data Fig. 3, and tissue from the remaining ChR2 mice showed similar expression patterns. Tissue from the only mouse that showed inconsistent (*i.e.*, no) levels of virus expression is also shown in the figure (Control 5). Extended Data Fig. 3 also shows representative images from all 4 mice injected with AAV5-hSyn-EYFP. Experiments with these AAV control mice were not conducted more than once. Behavioral experiments with WT mice were reproduced at a 6-month interval (Fig. 2, Extended Data Fig. 5). Histological and behavioral experiments attempting to drive Archaerhodopsin expression in the IO (Extended Data Fig. 1) were repeated over 3 years and consistently produced results similar to those shown in the figure.

Data collection and analysis were not performed blind to the conditions of the experiments. Our experimental design provided a within-animal control, and because comparisons were not required between different groups of mice, it was not necessary to be blind as to the group allocation of any individual mouse. In addition, analyses were based on automated scripts applied across experimental conditions and thus were not subject to any experimenter bias.

Data availability.

The data that support the findings of this study are available at www.github.com/blinklab/KimOhmaeMedina.

Code availability.

The code used to analyze the data in this study are available at www.github.com/blinklab/KimOhmaeMedina.

Extended Data

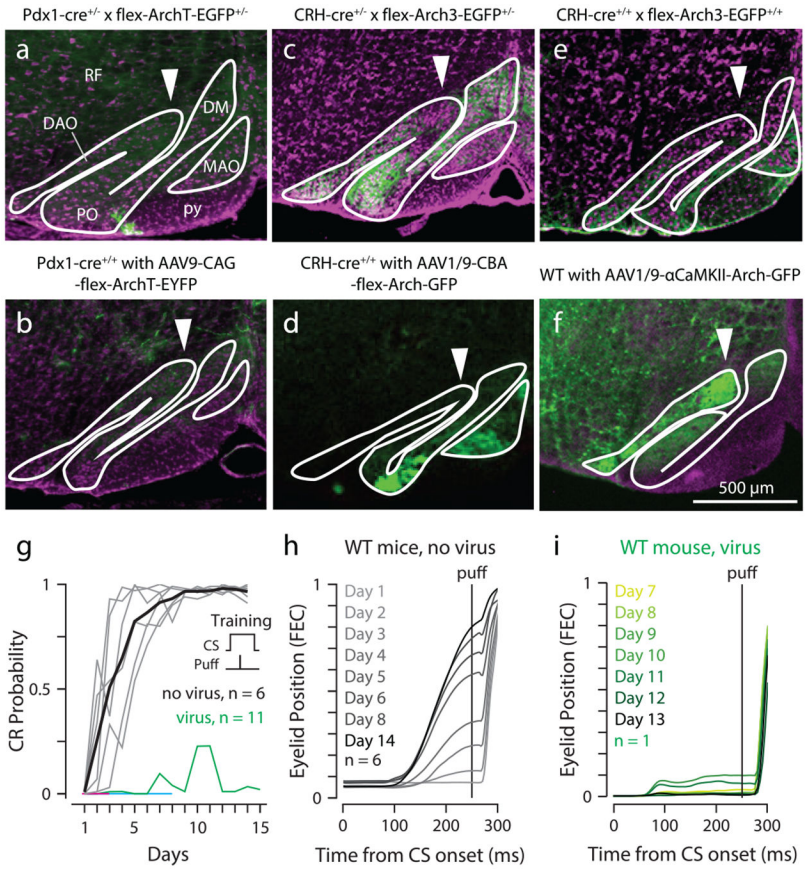

Extended Data Figure 1. Summary of failed experiments using inhibitory opsins in the dorsal accessory olive.

(**a**-**f**) Arch expression (green) in and around the IO (outlined in white) in histological sections counterstained with red fluorescent nissl (magenta). Expression of ArchT was very sparse and did not cover the region of the IO involved in eyeblink conditioning (dorsal accessory olive, DAO; white arrows) in Pdx-cre mice crossed with flex-ArchT mice (**a**), or Pdx-cre mice that received an AAV-ArchT injection in the IO (**b**). (**c**-**e**) Expression of Arch3 was patchy and did not cover the DAO in CRH-cre mice crossed with either heterozygous (**c**) or homozygous flex-Arch3 mice (**e**), or in CRH-cre mice that received an AAV-Arch injection in the IO (**d**). (**f**-**i**) Although we obtained good expression of Arch in the DAO in wildtype mice injected with AAV1/9-αCaMKII-Arch-GFP (**f**), the health of 8/11 mice began to deteriorate two weeks after AAV injection, such that the mice could not tolerate eyeblink conditioning sessions and had to be euthanized. Experiments were not possible in the few mice that survived (3/11 mice) because these mice were severely impaired in eyeblink conditioning (**g**), and the performance of even the best mouse (**i**) was much worse than the performance of control mice (**h**, control data previously published in[21]). Abbreviations: CR, conditioned response; CS, conditioned stimulus; DAO, dorsal accessory olive; DM, dorsomedial cell column; FEC, fraction eyelid closure; MAO, medial accessory olive; PO, principal olive; RF, reticular formation.

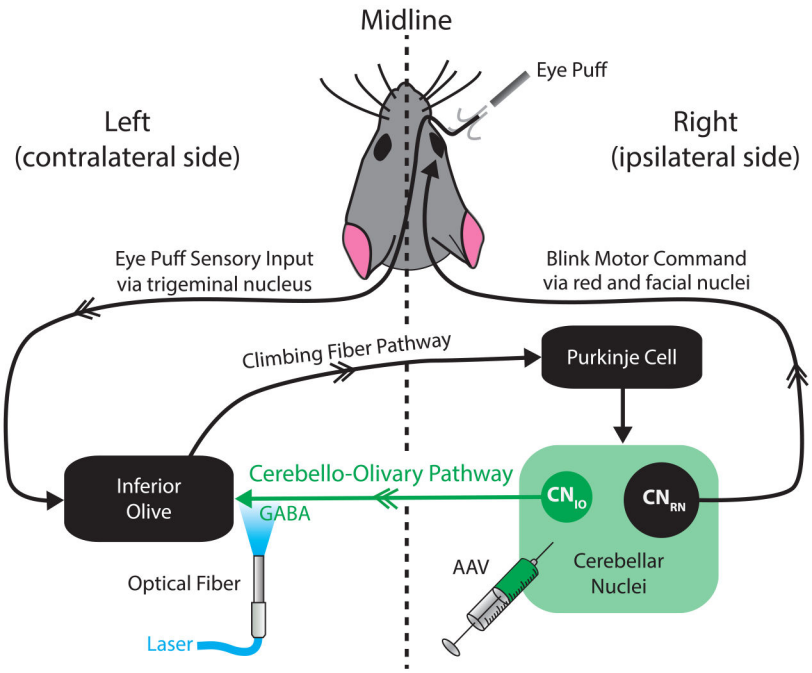

Extended Data Figure 2. Olivo-cerebellar circuits relevant to eyeblink conditioning.

Somatosensory information about the eye puff stimulus crosses the midline and is sent to the contralateral inferior olive via the trigeminal nucleus. The inferior olive sends a predominantly contralateral projection to eyeblink-generating Purkinje cells in the cerebellar cortex via the climbing fiber pathway. Purkinje cells and cerebellar nucleus projection (CN_{RN}) neurons control CR generation for the ipsilateral eye. Cerebellar nucleo-olivary neurons (CN_{IO}) send a GABAergic projection to the inferior olive. During the experiments described in this paper, we induced broad ChR2 expression in the cerebellar nuclei and then selectively activated the cerebello-olivary pathway by photostimulating CN_{IO} axon terminals at the level of the inferior olive. Note that CN_{IO} neurons are a distinct population, completely separate from the CN_{RN} neurons, and for this reason, photostimulation-driven backpropagating action potentials in the CN_{IO} axons do not have direct access to the neurons that are responsible for generating the eyeblink CR.

Extended Data Figure 3. Opsin expression and optical fiber placement in ChR2 and control mice.

(**a**, **e**) Outline of nuclei around the virus injection site (**a**) and the fiber implant site (**e**) traced from a representative mouse (ChR2 1). The cerebellar and inferior olivary nuclei implicated in eyeblink conditioning are highlighted in green (anterior interpositus nucleus, AIP; dorsal accessory olive; DAO) (**b**-**d**, **f**-**h**) Coronal sections at the level of the cerebellar nuclei (**b**-**d**) and inferior olive (**f**-**h**) from mice in the ChR2 (**b**, **d**, **f**, **h**) and control (**c**, **g**) groups. A unique identifier for each mouse is shown in the bottom left corner of each photomicrograph. Cerebellar and vestibular nuclei are revealed by fluorescent nissl stain (magenta). ChR2-EYFP (green) was visible at the level of the AIP (**b**-**d**) and, with longer exposure times, the DAO (**f**-**h**). The AAV injection did not work in mouse ‘Control 5’.

Lesions deliberately made at the end of the experiments to mark the location of the optical fiber tip are also visible just dorsal to the DAO (yellow dashed outline). Abbreviations: AIP, anterior interposed nucleus; cctx, cerebellar cortex; DAO, dorsal accessory olive; DM, dorsomedial cell column of the inferior olive; DC, dorsal cochlear nucleus; DN, dentate nucleus; F, fastigial nucleus; icp, inferior cerebellar peduncle; LVe, lateral vestibular nucleus; MAO, medial accessory olive; MVe, medial vestibular nucleus; P, paracochlear glial substance; PO, principal olive; py, pyramids; RF, reticular formation; VCB, vestibulocerebellar nucleus.

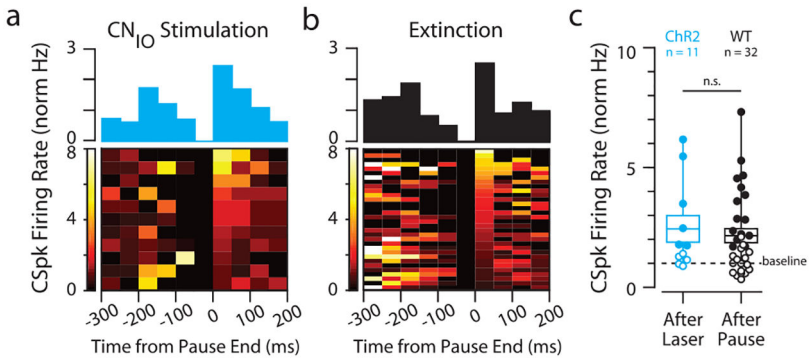

Extended Data Figure 4. CSpk activity is similar during CN$_{IO}$ stimulation and normal extinction.

(**a, b**) CSpk firing rate (normalized to pre-trial baseline) for individual neurons (heat plots) and for groups of neurons (mean, histograms) in 50-ms bins, aligned to the end of the pause during CN$_{IO}$ stimulation trials in ChR2 mice (**a**; $n = 11$ neurons, same as in Fig. 1l) or extinction trials in wildtype mice (**b**, $n = 32$ neurons, recorded during a previous experiment[5]). (**c**) Quantification of rebound size in the 50 ms after the pauses shown in (**a-b**). Each dot shows the mean, normalized firing rate response in the 50 ms after a pause (rebound window) for a single neuron. Dots are filled if neurons exhibited significant rebound firing (see Online Methods). Of the neurons recorded during CN$_{IO}$ stimulation trials in ChR2 mice, 6/11 (55%) exhibited a significant rebound. Of the neurons recorded during extinction trials in wildtype mice, 15/32 (47%) exhibited a significant rebound. There was no significant difference between rebound firing rates of the neurons recorded in the ChR2 and the wildtype mice ($n = 43$ neurons, two-sided Wilcoxon rank-sum test: $W = 195$, $p = 0.61$; boxplot center: mean, box bounds: ± SEM, whiskers: distribution minimum and maximum).

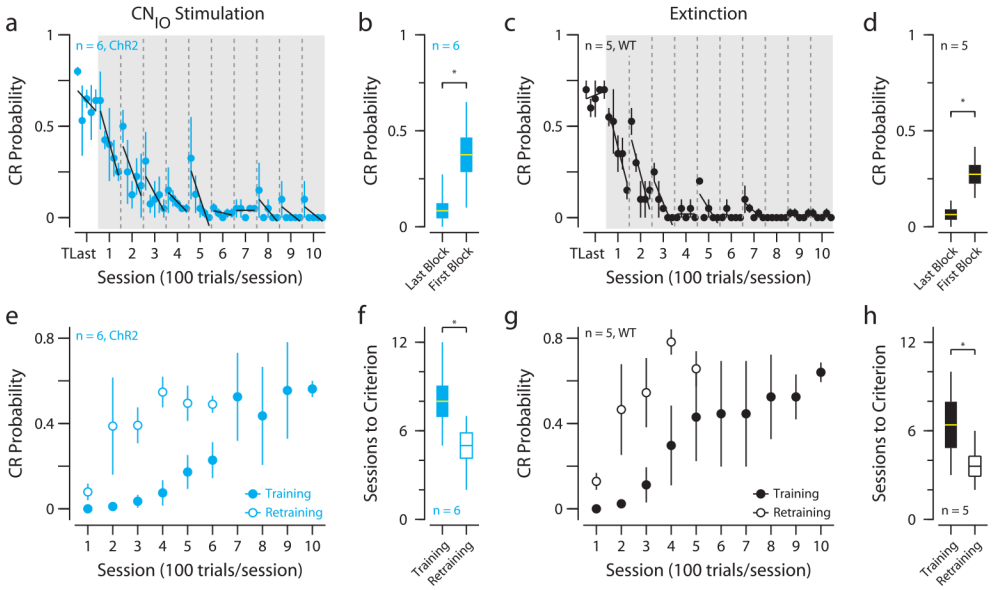

Extended Data Figure 5. Extinction during CN_{IO} stimulation displays spontaneous recovery and savings.

(**a**) CR probability (median ± MAD) measured in blocks of 20 trials during the final training session (white background) and repeated CN_{IO} stimulation sessions (gray shaded background) in ChR2 mice (n = 6 mice). Sessions are separated from each other by vertical dotted lines, and the line of best fit to the 5 median values in each session is shown. (**b**) CR probability in the last block of 10 trials in a session was significantly lower than in the first block of 10 trials in the next one for the first 5 sessions with CN_{IO} stimulation for the mice shown in panel **a** (n = 6 mice; two-tailed paired t-test: t = 3.63, df = 5, p = 0.015, d = 1.55). (**c**-**d**) Same as (**a**-**b**), but for wildtype mice undergoing extinction training (gray shaded background in panel **c**; n = 5 mice; two-tailed paired t-test: t = 5.53, df = 4, p = 0.005, d = 2.12). (**e**) CR probability (median ± MAD), and (**f**) number of sessions to acquire the task (mean ± SEM), during initial training (filled symbols) and retraining (open symbols) of ChR2 mice before and after CN_{IO} stimulation (n = 6 mice, training: 8 ± 1.06 sessions, retraining: 5 ± 0.86 sessions, one-tailed paired t-test: t = 3.22, df = 5, p = 0.01, d = 1.25). (**g**-**h**) Same as (**e**-**f**), but for initial training and retraining of wildtype mice before and after extinction (**h**, n = 5 mice, training: 6.5 ± 1.6 sessions, retraining: 3.6 ± 0.68 sessions, one-tailed paired t-test: t = 2.62, df = 4, p = 0.03, d = 0.67). Family-wise alpha values were Bonferroni-Holm corrected for multiple comparisons. In panels **b**, **d**, **f**, **h**, boxplot center: mean, box bounds: ± SEM, whiskers: distribution minimum and maximum. * p < 0.05.

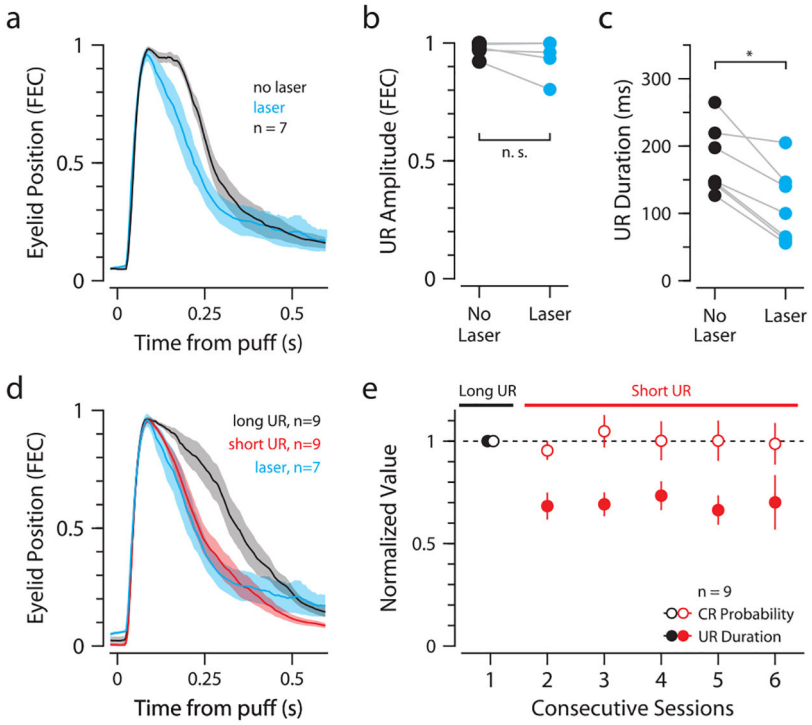

Extended Data Figure 6. Extinction during CN_{IO} stimulation is not caused by impaired processing of eye puff stimulus.

(**a**) Averaged reflex eyelid responses to the airpuff (unconditioned response, UR; mean ± SEM). (**b**) UR peak amplitude ($n = 7$ mice; two-tailed paired t-test: $t = 1.41$, $df = 6$, $p = 0.21$), and (**c**) UR duration in sessions with (blue) and without (black) CN_{IO} stimulation for ChR2 mice ($n = 7$ mice; two-tailed paired t-test: $t = 5.51$, $df = 6$, $p = 0.001$, $d = 1.25$). Only trials without eyelid movements preceding the airpuff are included. (**d**) URs (mean ± SEM) from 9 mice, during training sessions in which the intensity of the eye puff was systematically changed to generate long URs (black) or short URs (red). URs during CN_{IO} stimulation sessions in (**a**) are duplicated for comparison (blue). (**e**) CR probability (open circles) and UR duration (filled circles; mean ± SEM) for the mice in (**d**), shown during a training session with long URs (black) and the following 5 consecutive training sessions, in which the eye puff intensity was set to generate shorter URs (red). In spite of shorter URs (filled red circles; $n = 9$ mice, Friedman's ANOVA: $F_r = 12.71$, $df = 4$, $p = 0.013$, $W = 0.35$), CR probability remained unchanged (open red circles; $n = 9$ mice, Friedman's ANOVA: $F_r = 5.07$, $df = 4$, $p = 0.28$). Family-wise alpha values were Bonferroni-Holm corrected for multiple comparisons. * $p < 0.05$.

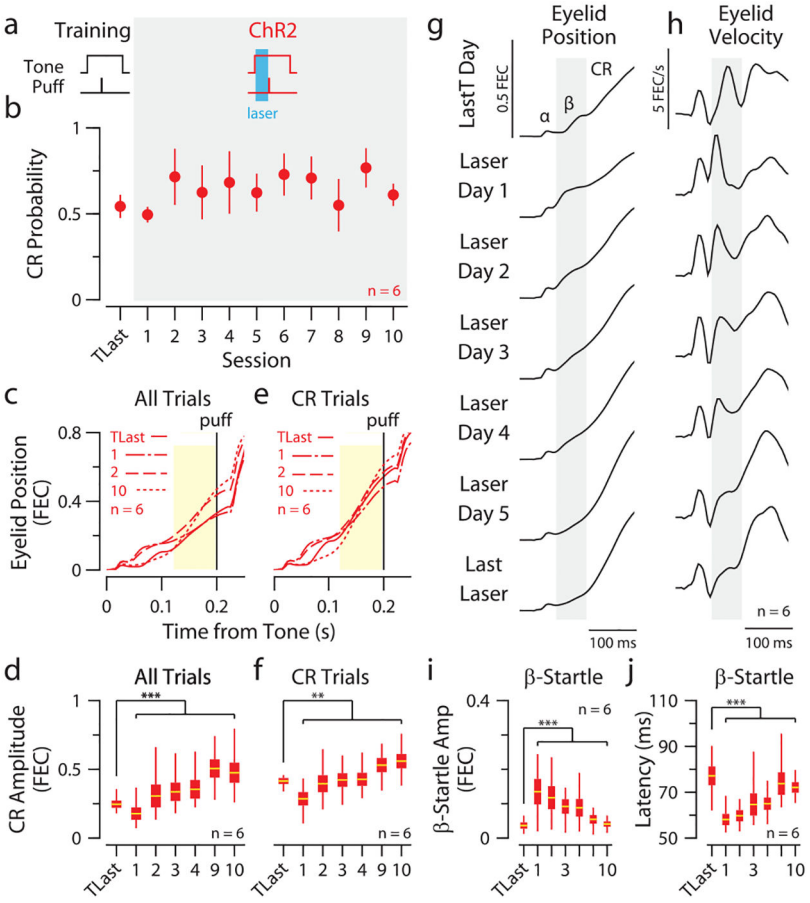

Extended Data Figure 7. CN_{IO} stimulation before the airpuff does not impair CR performance. (**a**) Schematic showing relative timing of stimulus presentations and laser pulses in the different phases of the experiment. (**b**) CR probability (median ± MAD) in the last training session ('TLast') and sessions during CN_{IO} stimulation (gray shaded area) in ChR2 mice (n = 6 mice; CR probability increased during CN_{IO} stimulation, Friedman's ANOVA: F_r = 14.86, df = 6, p = 0.02, W = 0.36). (**c**) Averaged eyelid movement traces, and (**d**) CR amplitude during sessions with CN_{IO} stimulation increased significantly (n = 6 mice; Friedman's ANOVA: F_r = 24.50, df = 6, $p = 4.22 \times 10^{-4}$, W = 0.68). Repeating the analysis in (**c-d**) but excluding trials without CRs revealed that the increase in CR amplitude during CN_{IO} stimulation shown in (**d**) is not simply driven by a higher CR probability – CRs were significantly larger (**e-f**; n = 6 mice; Friedman's ANOVA: F_r = 20.0, df = 6, p = 0.003, W = 0.56). The time window used to calculate CR amplitude is indicated (**c, e**; yellow shaded area). (**g**) Averaged eyelid position, and (**h**) eyelid velocity traces for the last training session and subsequent sessions with CN_{IO} stimulation. The gray shaded area highlights the β-startle window, which follows the α-startle and precedes the CR. (**i**) β-startle amplitude was increased (n = 6 mice; Friedman's ANOVA: F_r = 29.71, df = 6, $p = 4.45 \times 10^{-5}$, W = 0.82), and (**j**) latency was shortened (n = 6 mice; Friedman's ANOVA: F_r = 25.57, df = 6, $p = 2.67 \times 10^{-4}$, W = 0.71) excluding trials without a β-startle. Family-wise alpha was Bonferroni-Holm adjusted for multiple comparisons. In panels **d**, **f**, **i**, **j**, boxplot center: mean, box

bounds: ± SEM, whiskers: distribution minimum and maximum). ** $p < 0.01$, *** $p < 0.001$.

ACKNOWLEDGMENTS

Supported by grants to JFM from the National Institutes of Health (R01 MH093727; RF1 MH114269; NIH R01NS112917), and a grant to OAK (F31 NS103427). We thank Shane Heiney for help with surgical approach and Jenni Siegel for help with analysis.

REFERENCES

1. Schultz W & Dickinson A Neuronal coding of prediction errors. Annu Rev Neurosci 23, 473–500 (2000). [PubMed: 10845072]
2. Dunsmoor JE, Niv Y, Daw N & Phelps EA Rethinking Extinction. Neuron 88, 47–63 (2015). [PubMed: 26447572]
3. Mauk MD & Donegan NH A model of Pavlovian eyelid conditioning based on the synaptic organization of the cerebellum. Learn Mem 3, 130–158 (1997).
4. Rasmussen A, Jirenhed DA & Hesslow G Simple and complex spike firing patterns in Purkinje cells during classical conditioning. Cerebellum 7, 563–6 (2008). [PubMed: 18931885]
5. Ohmae S & Medina JF Climbing fibers encode a temporal-difference prediction error during cerebellar learning in mice. Nat Neurosci 18, 1798–803 (2015). [PubMed: 26551541]
6. Medina JF, Nores WL & Mauk MD Inhibition of climbing fibres is a signal for the extinction of conditioned eyelid responses. Nature 416, 330–3 (2002). [PubMed: 11907580]
7. McCormick DA, Steinmetz JE & Thompson RF Lesions of the inferior olivary complex cause extinction of the classically conditioned eyeblink response. Brain Res 359, 120–130 (1985). [PubMed: 4075140]
8. Bengtsson F, Jirenhed DA, Svensson P & Hesslow G Extinction of conditioned blink responses by cerebello-olivary pathway stimulation. Neuroreport 18, 1479–82 (2007). [PubMed: 17712278]
9. Zbarska S, Bloedel JR & Bracha V Cerebellar dysfunction explains the extinction-like abolition of conditioned eyeblinks after NBQX injections in the inferior olive. J Neurosci 28, 10–20 (2008). [PubMed: 18171918]
10. Ruigrok TJ & Teune TM Collateralization of cerebellar output to functionally distinct brainstem areas. A retrograde, non-fluorescent tracing study in the rat. Front Syst Neurosci 8, 23 (2014). [PubMed: 24600356]
11. Freeman JH & Steinmetz AB Neural circuitry and plasticity mechanisms underlying delay eyeblink conditioning. Learn Mem 18, 666–77 (2011). [PubMed: 21969489]
12. Najafi F & Medina JF Beyond “all-or-nothing” climbing fibers: graded representation of teaching signals in Purkinje cells. Front Neural Circuits 7, 115 (2013). [PubMed: 23847473]
13. Salinas-Hernandez XI et al. Dopamine neurons drive fear extinction learning by signaling the omission of expected aversive outcomes. Elife 7 (2018).
14. Chang CY et al. Brief optogenetic inhibition of dopamine neurons mimics endogenous negative reward prediction errors. Nat Neurosci 19, 111–6 (2016). [PubMed: 26642092]
15. Lee K et al. Temporally restricted dopaminergic control of reward-conditioned movements. Nat Neurosci 23, 209–216 (2020). [PubMed: 31932769]
16. Bayer HM & Glimcher PW Midbrain dopamine neurons encode a quantitative reward prediction error signal. Neuron 47, 129–41 (2005). [PubMed: 15996553]
17. Wagner MJ, Kim TH, Savall J, Schnitzer MJ & Luo L Cerebellar granule cells encode the expectation of reward. Nature 544, 96–100 (2017). [PubMed: 28321129]
18. Ernst TM et al. The cerebellum is involved in processing of predictions and prediction errors in a fear conditioning paradigm. Elife 8 (2019).
19. Popa LS, Streng ML, Hewitt AL & Ebner TJ The Errors of Our Ways: Understanding Error Representations in Cerebellar-Dependent Motor Learning. Cerebellum 15, 93–103 (2016). [PubMed: 26112422]

20. Brooks JX, Carriot J & Cullen KE Learning to expect the unexpected: rapid updating in primate cerebellum during voluntary self-motion. Nat Neurosci 18, 1310–7 (2015). [PubMed: 26237366]

21. Heiney SA, Wohl MP, Chettih SN, Ruffolo LI & Medina JF Cerebellar-dependent expression of motor learning during eyeblink conditioning in head-fixed mice. J Neurosci 34, 14845–53 (2014). [PubMed: 25378152]

22. Deisseroth K Predicted irradiance values: model based on direct measurements in mammalian brain tissue. https://web.stanford.edu/group/dlab/cgi-bin/graph/chart.php (2012).

23. Kehoe EJ Repeated acquisitions and extinctions in classical conditioning of the rabbit nictitating membrane response. Learn Mem 13, 366–75 (2006). [PubMed: 16705135]

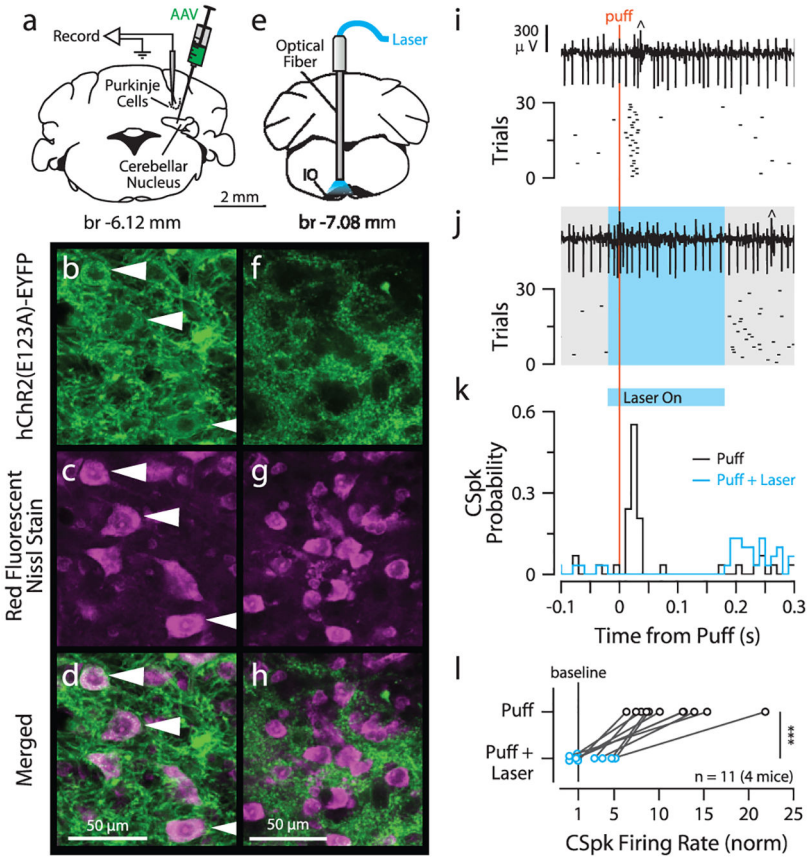

Figure 1. Inhibiting the IO *in vivo*.

(**a-h**) Analysis of opsin expression in the sites of AAV-hSyn-ChR2-EYFP injection in the cerebellar nuclei (**a-d**), and optical fiber implant in the IO (**e-h**). Confocal images from one example mouse (from $n = 11$ total mice), showing ChR2-EYFP expression (green) in somata of cerebellar nucleus neurons (**b**, arrow head) and CN_{IO} terminal axons in the IO (**f**). Fluorescent Nissl stain (magenta) indicates location of cell bodies in the cerebellar nucleus (**c, d**) and IO (**g, h**). (**i**, **j**) (Top) Raw extracellularly recorded signals showing simple spikes and complex spikes (CSpks, ^) from an example trial. (Bottom) CSpk raster plots for an example Purkinje cell for control condition (**i**) and during photostimulation of CN_{IO} terminals in the IO (**j**, blue shading; 11.63 mW/mm^2, 200 ms laser pulse starting 20 ms before the airpuff trigger). (**k**) Peristimulus time histograms (bin size = 10 ms) for the CSpks in the two raster plots of **i-j**. (**l**) Suppression of CSpk responses to airpuff by CN_{IO} stimulation (blue) ($n = 11$ neurons from 4 mice; two-tailed paired t-test: $t = 6.54$, $df = 10$, $p = 6.56 \times 10^{-5}$, $d = 2.58$). CSpk rates were normalized to pre-trial baseline. *** $p < 0.001$.

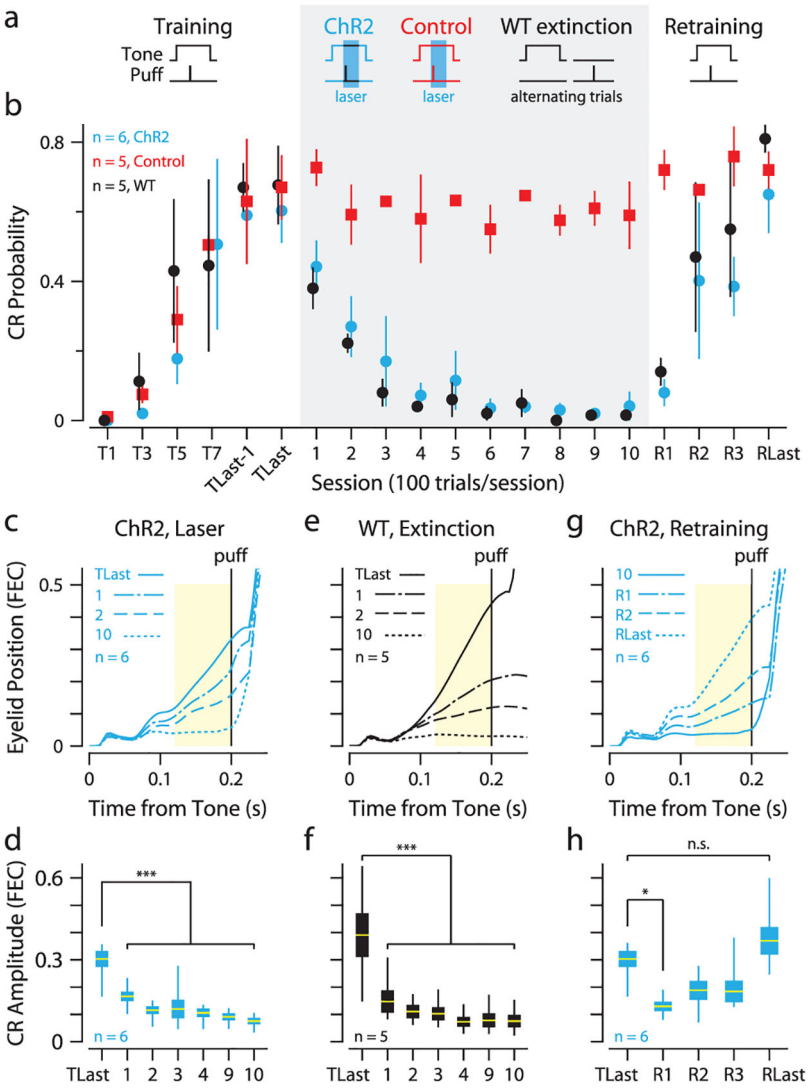

Figure 2. CN_{IO} stimulation during eye puff stimulus.

(**a**) Schematic showing the relative timing of stimulus presentations and laser pulses in the different phases of the experiments. (**b**) CR probability (median ± MAD) before (left, 'Training'), during (gray shaded area), and after (right, 'Retraining') the sessions with optogenetic stimulation in ChR2 (blue circles, $n = 6$ mice, reduction in CR probability was significant: Friedman's ANOVA: $F_r = 32.17$, $df = 6$, $p = 1.51 \times 10^{-5}$, $W = 0.81$) and control (red squares, $n = 5$ mice, no change in CR probability: Friedman's ANOVA: $F_r = 5.23$, $df = 6$, $p = 0.51$) groups, or sessions with extinction in the wildtype group (*$n = 5$ mice*, black circles). An nparLD analysis showed that the ChR2 and WT mice exhibited no differences in their learning rates ($n = 10$ mice, nparLD, $F_{group*session} = 1.56$, $df = 2.40$, $p = 0.20$). After the laser manipulation, mice in the ChR2 group produced very few CRs ('Retraining', mean ± SEM, 1.7 ± 1.1 CRs in the first 10 trials). (**c**, **e**, **g**) Averaged eyelid movement traces, and (**d**, **f**, **h**) CR amplitude during the 'laser' phase for ChR2 mice (**c-d**; $n = 6$ mice; Friedman's ANOVA: $F_r = 26.14$, $df = 6$, $p = 2.09 \times 10^{-4}$, $W = 0.73$), during the extinction phase for wildtype mice (**e-f**; $n = 5$ mice; Friedman's ANOVA: $F_r = 19.54$, $df = 6$, $p = 3.34 \times 10^{-3}$, W

= 0.65), and during the 'Retraining' phase for ChR2 mice (**g-h**). In (**h**), two-tailed paired t-tests showed a significant difference between CR amplitudes on the last day of training and the first day of re-training ($n = 6$ mice, $t = 8.05$, $df = 5$, $p = 4.79 \times 10^{-4}$, $d = 2.60$) but no difference between the last day of training and last day of re-training ($n = 6$ mice, $t = -0.35$, $df = 5$, $p = 0.74$). The time window used to calculate CR amplitude is indicated (**c, e, g**; yellow shaded area). In all panels, boxplot center: mean, box bounds: ± SEM, whiskers: distribution minimum and maximum. Family-wise alpha values were Bonferroni-Holm corrected for multiple comparisons. * $p < 0.05$, *** $p < 0.001$.

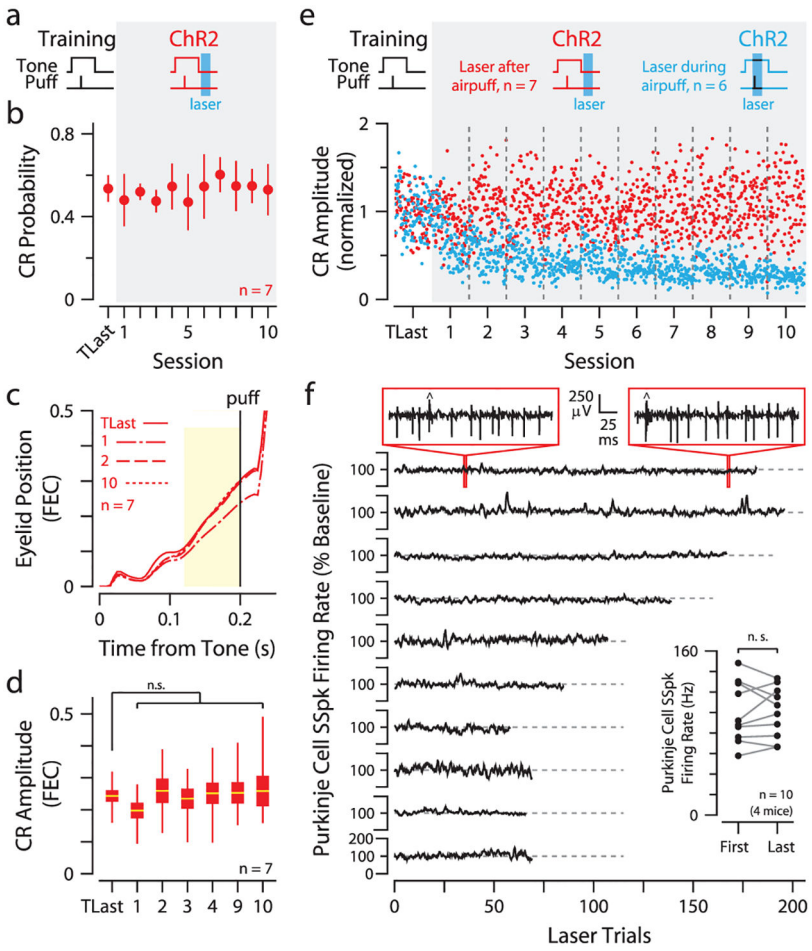

Figure 3. CN_{IO} stimulation after eye puff stimulus.

(**a**) Schematic showing the relative timing of stimulus presentations and laser pulses in the different phases of the experiment. (**b**) CR probability (median ± MAD, $n = 7$ mice, no change in CR probability: Friedman's ANOVA: $F_r = 1.40$, $df = 7$, $p = 0.97$), (**c**) averaged eyelid movement traces, and (**d**) CR amplitude were unchanged during sessions with CN_{IO} stimulation delivered after the airpuff in ChR2 mice ($n = 7$ mice; Friedman ANOVA: $F_r = 1.41$, $df = 7$, $p = 0.96$; boxplot center: mean, box bounds: ± SEM, whiskers: distribution minimum and maximum). (**e**) Comparison between the averaged trial-by-trial changes in CR amplitude (normalized to mean CR amplitude on 'TLast') in the 'Laser after airpuff' experiment (red) and the 'Laser during airpuff' experiment shown in Fig. 2 (blue, $n = 6$ mice). Individual sessions are separated from each other by vertical dashed lines. The time window used to calculate CR amplitude is indicated (**c**; yellow shaded area). (**f**) Raw extracellular signal (red boxes; CSpk ^) and simple spike firing rate during repeated trials with CN_{IO} stimulation for 10 Purkinje cells (same cells as Fig. 1; firing rate normalized to the mean in the first 5 trials, filtered using a moving average with window size of 1 trial). (**f**, inset) Simple spike firing rate during the first 10% ('First') and last 10% ('Last') of trials in the recording session for each cell ($n = 10$ neurons; two-tailed paired t-test: $t = -0.14$, $df = 9$,

$p = 0.89$). Family-wise alpha values were Bonferroni-Holm corrected for multiple comparisons.